

Improvement of Electrochemical Trepanning by Using a Pictographic Insulation Sleeve

Gu Zhouzhi¹, Zhu Dong^{1,2,*}, Xue Tingyu¹, Liu Ao¹, Zhu Di^{1,2}

¹ College of Mechanical and Electrical Engineering, Nanjing University of Aeronautics and Astronautics, Nanjing, China, 210016

² Jiangsu Key Laboratory of Precision and Micro-Manufacturing Technology, Nanjing, China, 210016

*E-mail: zhudong@nuaa.edu.cn

Received: 14 July 2017 / *Accepted:* 12 September 2017 / *Published:* 12 October 2017

Electrochemical trepanning is an economical approach for machining straight blades made of hard to cut materials. However, the stray corrosion caused by cathode tip in traditional electrochemical trepanning process, may introduce a tapered wall of fabricated blade. In this paper, a modified electrochemical trepanning process with a pictographic insulation sleeve based on the lateral flow mode is proposed to reduce the taper of blade. Computer-aided optimization method was investigated to optimize the protruding length of pictographic insulation sleeve. Finally, a series of experiments were carried out and results showed that the taper angle of fabricated blade has been reduced from 0.286° to 0.106°, when protruding length of the pictographic insulation sleeve improved from 0 to 0.4 mm.

Keywords: electrochemical trepanning, lateral flow, pictographic insulation sleeve, stray corrosion, taper

1. INTRODUCTION

To achieve higher thermal efficiency in aero engines, nickel-based super alloy has been widely used in the manufacture of aero engine components. Due to its hard-to-cut nature, the traditional machining process of nickel-based super alloy has reached the economic limit. Compared with traditional machining techniques, electrochemical machining (ECM) is a promising and low-cost process to machine these hard-to-cut materials due to its unique material removal mechanism. During the process of ECM, a cathode tool and the anode workpiece are immersed in an electrolytic solution, and material is removed by electrochemical reaction when a potential difference is applied between the opposing electrodes. Moreover, ECM is superior in a number of ways, including high material removal

rate and absence of tool wear and metallurgical defects. Because of these properties, ECM has been widely used in the field of machining of aero engine components, which are commonly composed of hard-to-cut materials [1-5].

ECM is the predominant process for machining the blades of aero engines due to its ability to meet the high surface quality demands of aero engine components. Zhu introduced a new cathode design method based on iterative correction of predicted profile errors in blade ECM [6]. Toshiaki proposed an advanced integrated approach for 3D simulations of the aero engine blade [7]. Klocke presented a modeling and simulation method of the material removal process for the ECM machining of blades and blisks [8]. To meet the application potential, many researchers have focused on the investigation of improving profile accuracy and surface quality of components machined by ECM. Zaytsev studied the formation mechanism of jet-defect aligned along the electrolyte stream and investigated the effect of flow field cavitations on machining accuracy of ECM [9]. Bilgiet proposed an ECM process with a rotating electrode to reduce or eliminate the flow field disruption and enhance the machining accuracy of the workpiece [10]. Burger investigated the influence of chemical composition, microstructure and homogeneity on the electrochemical dissolution behavior and surface quality of a workpiece made of nickel-based super alloy [11]. Rosenkranz investigated the influence of pulse length and prepolarisation of electrode on the surface structure during pulsed ECM [12].

Stray corrosion is a critical issue in the ECM process which affects the machining accuracy and surface quality. To limit the stray corrosion effect during the ECM process, a series of novel approaches have been proposed by researchers. Jain investigated the stray current attack and stagnation zones in electrochemical drilling, and obtained good dimensional accuracy by using bits as the cathode in ECM [13]. Fang presented a new method in which a potential difference was applied between an auxiliary electrode and the workpiece anode to diminish the stray corrosion at the hole exit [14]. Chen introduced a thick mask in through-mask electrochemical micro-machining to prevent the escape of oxygen bubbles from the micro-dimples. By utilizing oxygen bubbles generated during the machining process, the lateral undercutting caused by stray corrosion can be reduced [15].

Stray corrosion caused by the cathode tip is an inherent issue in the electrochemical trepanning process, which may result in a tapered blade. In this paper, a pictographic insulation sleeve is applied to decrease the taper of fabricated blade by restricting the region affected by stray corrosion.

2. PRINCIPLE AND ANALYSIS

In the electrochemical trepanning process, forward flow is usually adopted for its simple cathode structure and convenience of tool installation. A traditional trepanning process with forward flow is schematically illustrated in Fig. 1. The assembled cathode consists of a cathode base and cathode tip, and the insulation coating covers the internal surface of the cathode base. During the machining process, the electrolyte is pumped from the cathode internal hollow and flows through the side gap Δ_s and frontal gap Δ_b (Fig. 1a). When a potential difference is applied to the anode and cathode, material removal takes place at the anode surface. As the cathode feeds toward the anode, the blade is formed in the cathode hollow. However, surface of blade is suffered from the stray corrosion

during machining process, which will result in a tapered blade. The taper is relevant to the impact time of stray current. The shorter impact time is beneficial for a smaller taper. The impact time T_i can be calculated from formula (1):

$$T_i = \frac{H}{V_f} \tag{1}$$

Where, H is the impact height of stray current, V_f is the feeding rate of cathode.

To decrease the taper, high feeding rate is usually applied in traditional trepanning process to shorten the impact time of stray current. However, when feeding rate V_f is increased, the side gap Δ_s will become narrow, which may deteriorate the machining stability.

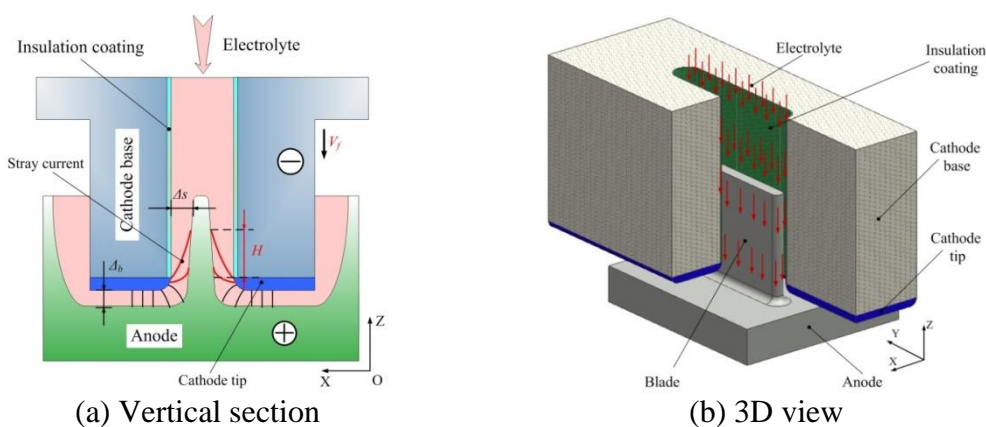


Figure 1. Traditional trepanning process based on forward flow

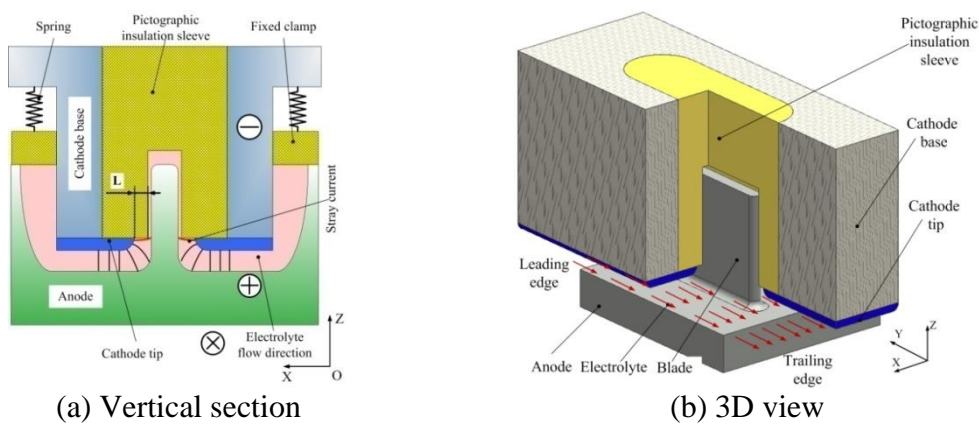


Figure 2. Modified trepanning process with pictographic insulation sleeve

As our previous work shows, a lateral flow mode can weaken the electrolyte flow at side gap and allows the processing products gathering at the side gap, which is help to decrease the blade taper. However, the improvement is very limited by only change the flow mode. In this paper, a modified trepanning process with a pictographic insulation sleeve based on the lateral flow mode is proposed to decrease the taper by shortening the impact height H of stray current without change the feeding rate (Fig. 2). By adjusting the protruding length L (Fig. 2a), the sleeve becomes very close to the blade, the impact height H is reduced to a very small value. The distance H is decreased means that the impact

time T_i of stray current is limited, which can decrease the taper of fabricated blade. In this modified trepanning process, lateral flow mode is selected. The electrolyte flows from the leading edge to trailing edge (Fig. 2b), so the change of protruding length L has no influence on flow field in the front gap, and the machining stability can be ensured.

3. COMPUTER-AIDED OPTIMIZATION METHOD AND SIMULATION

3.1 Computer-aided optimization method

Design of the protruding length L of pictographic insulation sleeve is a major work of the modified trepanning process. To efficiently limit the stray corrosion, the sleeve should be very close to the blade, so the protruding length L should be coordinate with the side gap Δ_s . Because the side gap will change with the protruding length, a computer-aided optimization method is applied to accurately design the protruding length L . In the optimization process, protruding length L is the design variable, distance D (Fig. 3) between sleeve wall and blade wall is the target variable.

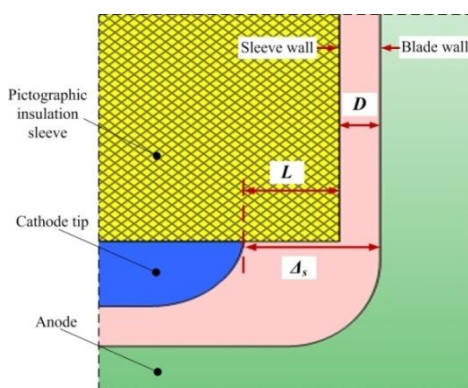


Figure 3. Illustration of gap distribution

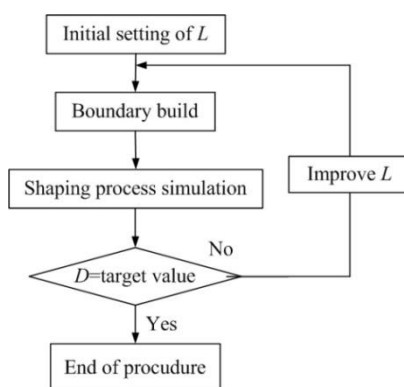


Figure 4. Diagram of optimization procedure

The optimization procedure was built by Ansys Parametric Design Language (APDL), and diagram of it is shown in Fig. 4. As is shown in the figure, the optimization procedure includes four

steps: (1) The initial value of protruding length L is set up. (2) The initial boundary for simulation is built according the given length L . (3) Shaping process of electrochemical trepanning is simulated by finite element method (FEM). (4) The distance D between sleeve wall and blade wall is checked after shaping process simulation. If D reaches the target value, optimization procedure is ended. Otherwise, above-mentioned steps will be repeated until D reaches the target value.

An example of the initial boundary for simulation is shown in Fig. 5. Γ_1 is the boundary of workpiece, Γ_4 and Γ_5 are the cathode boundaries. $\Gamma_6, \Gamma_7, \Gamma_8$ and Γ_9 are the boundaries of insulation sleeve, and the length of Γ_6, Γ_7 denotes the protruding length L . Γ_2, Γ_3 and Γ_{10} are the vertical boundaries, and the length of Γ_2, Γ_3 denotes the initial machining gap.

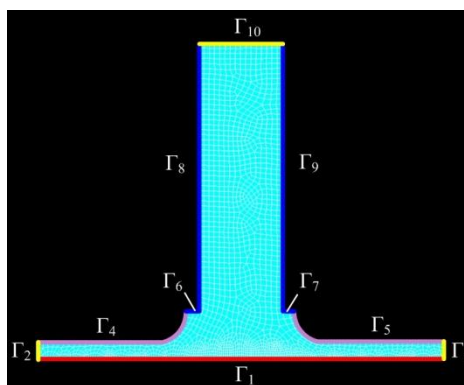


Figure 5. Example of the initial boundary for simulation

In the simulation process, the boundaries were frequently updated. Boundaries $\Gamma_2 - \Gamma_{10}$ move in the Z direction (Fig. 6), and the velocity is equal to the cathode feed rate V_f . Boundary Γ_1 evolves according to the material removal rate V_r of each node at the boundary, which can be calculated by Faraday's Law:

$$V_r = \eta \omega \cdot i \tag{2}$$

Where η is the current efficiency, ω is the volumetric electrochemical equivalent of the material, i is the current density.

When apply sodium nitrate solution to machining the material Inconel 718, current efficiency η can be obtained by following formula [16]:

$$\eta = 0.26e^{-i/8.4} + 0.66 \tag{3}$$

Current density i equals the product of electric field intensity E and electric conductivity κ :

$$i = \kappa \cdot E \tag{4}$$

The electric field can be obtained by simulation. In order to simplify the electric model, the following additional assumptions have been made in developing the mathematical model of the electrochemical trepanning process: (1) The electrical conductivity is constant in the gap. (2) The polarization potential is constant in the gap. (3) The electric field in the gap is quasi-stationary. Based on the assumptions, the electric potential ϕ in the mathematical model can be approximately described by Laplace's equation:

$$\nabla^2 \varphi = 0 \tag{5}$$

Table 1. Parameters of simulation process

Parameters	Setting
Volumetric electrochemical equivalent ω	2.09 mm ³ /A · min
electric conductivity κ	0.015 s/mm
Potential difference U	20 V
Feeding rate V_f	2 mm/min
Feeding depth	10 mm
Time interval	0.1 s

Based on above mentioned equations, the electrochemical trepanning process is simulated. The parameters setting are shown in Table 1. Fig. 6 shows a diagrammatic representation of the boundary evolutions in the simulation process of a certain L .

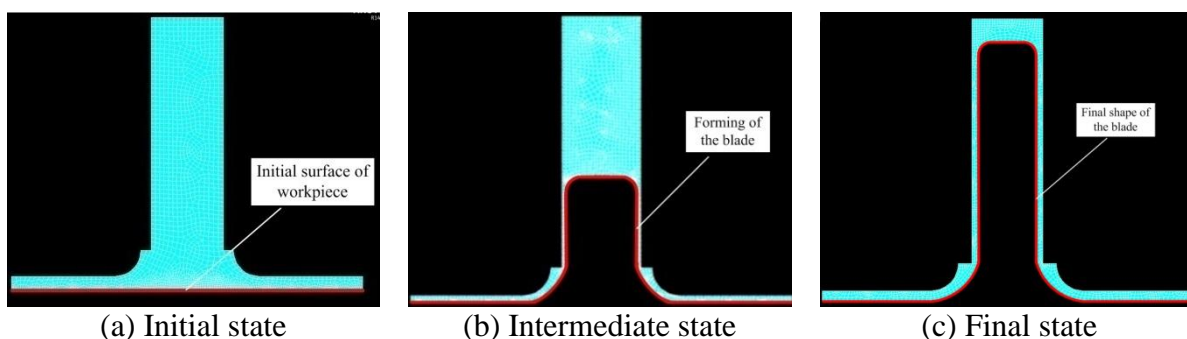


Figure 6. Diagrammatic representation of the boundary evolutions

3.2 Simulation

Parameters setting of the optimization procedure are shown in Table 2. The initial value of protruding length L is 0, the increase step of L is 0.05 mm. To effectively shield stray current as well as avoid motion interference between the pictographic insulation sleeve and blade, the target value of D is set up to 0.05±0.01 mm. The procedure starts with the initial value of 0, and ends after 9 iterations when L is 0.4mm.

During the optimization procedure, dimensions of distance D (between sleeve wall and blade wall) and side gap Δ_s changes with protruding length L , which are shown in Fig. 7. It is clear from the figure that distance D decreases as protruding length L is improved, and reaches 0.049 mm when protruding length L is improved to 0.4mm, which meets the demand of optimization. As the variation curve of side gap Δ_s with protruding L shows, the side gap Δ_s decreases gradually from 0.517 mm to

0.449 mm, when protruding length L is improved from 0 mm to 0.4 mm. The drop of side gap denotes that the stray corrosion has been reduced by the pictographic insulation sleeve.

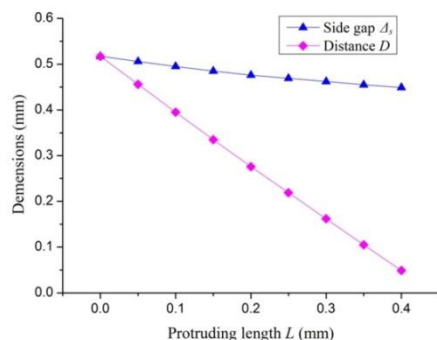


Figure 7. Variation of distance D and side gap Δ_s with protruding length L

Distributions of current density in inter-electrode before and after optimization are shown in Fig. 9. Before optimization, blade wall upon the cathode tip is still suffered from the stray current when protruding length L is 0 mm (Fig. 9a), which will introduce stray corrosion on and result in tapered blade. After optimization, stray current is cut off by the pictographic insulation sleeve with the optimized protruding length of 0.4 mm (Fig. 9b), so the stray corrosion region is nearly restricted.

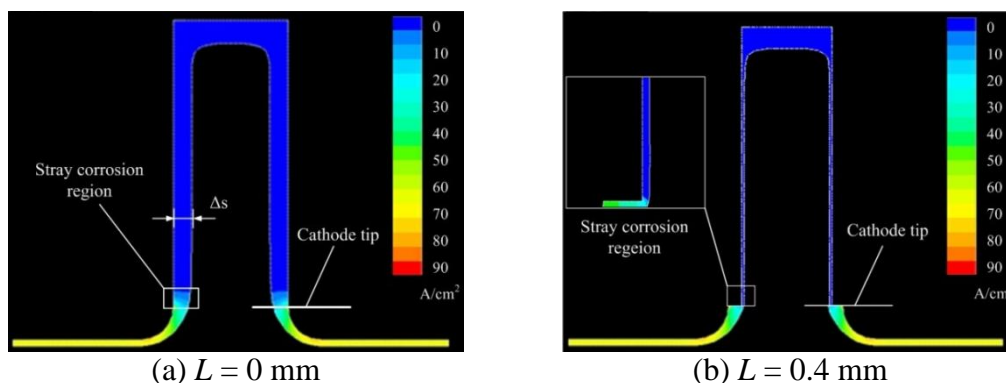


Figure 8. Distributions of current density in inter-electrode

Variation of current density at the blade wall is drawn in Fig.9. It can be seen from the figure that the current density at the blade wall gradually decreases with the height from the cathode tip. The current density approaches minimal value of 0 A/cm² at the height of 2.31 mm, which can be defined as the impact height H of stray current. Fig. 10 reveals that the protruding length is a significant factor that influences the impact height. As protruding length increases, the impact height decreases rapidly. When protruding length L is improved to 0.4 mm, the impact height H decreases to only 0.21mm. The great drop of impact height H means that the impact time T_i of stray current is well limited, and a blade with smaller taper can be obtained.

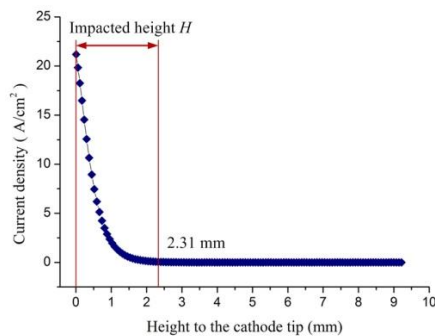


Figure 9. Variation of current density at blade wall

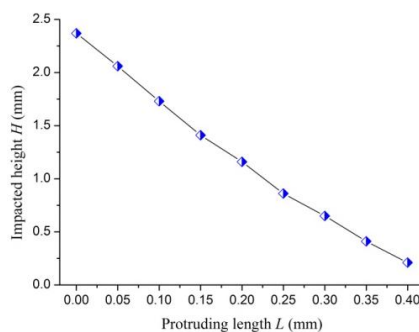


Figure 10. Variation of H with protruding length

4. RESULTS AND DISCUSSION

To confirm the practicality of the proposed modified trepanning process, a series of experiments were carried out by different pictographic insulation sleeves respectively with protruding length L of 0mm, 0.2mm and 0.4 mm. Sodium nitrate solution was selected as the electrolyte, which was pumped into the machining gap from the leading edge. The electrolyte temperature is 30°C, and inlet pressure is 1.2 MPa. Combined clamps were applied to restrict flow direction and prevent leakage of electrolyte. Cathode moved along the feeding direction with rate of 2 mm/min. The apparatus for the modified electrochemical trepanning process are shown in Fig. 11. The parameters of the experiments are shown in Table 2.

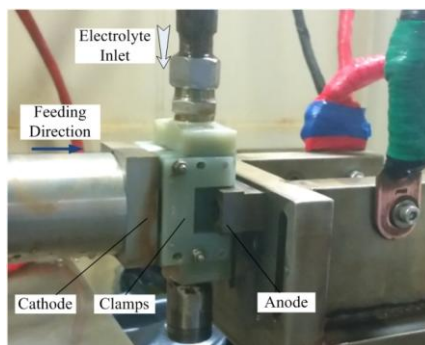


Figure 11. Apparatus of the experiments

Table 2. Parameters of the experiments

Conditions	Setting
Workpiece material	Inconel 718
Electrolyte composition	20 % NaNO ₃
Electrolyte temperature	30 °C
Electrolyte pressure	1.2 M Pa
Feed rate	2 mm/min
Potential difference	20 V

During experiments, the machining current was recorded and shown in Fig. 12. When *L* is set up as 0 mm, machining current rises rapidly from 213A to 811A in first 2 mm of the feeding depth, and rises gradually to the maximum value of 878A at the end of machining process. The same variations trend of machining current can be seen in process with protruding length *L* of 0.2mm and 0.4 mm. The maximum value of machining current is 874 A and 862A, when protruding length *L* is 0.2mm and 0.4 mm respectively. Declines of the maximum value of machining current have been detected in the machining process, which is attributed to the decrease of stray corrosion. In ECM variation of current can reflect the change in interelectrode gap [17]. Fluctuation was not observed in the current curve, which reveals that the improvement of protruding length has no influence on machining stability. The Machined samples of the experiments are shown in Fig. 13.

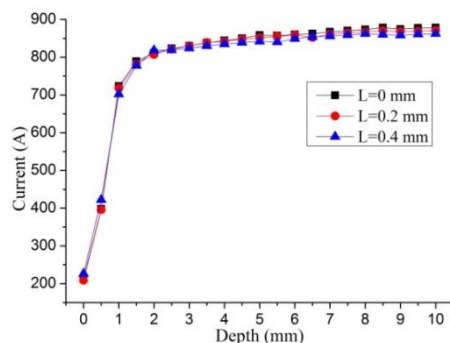


Figure 12. Variation of machining current

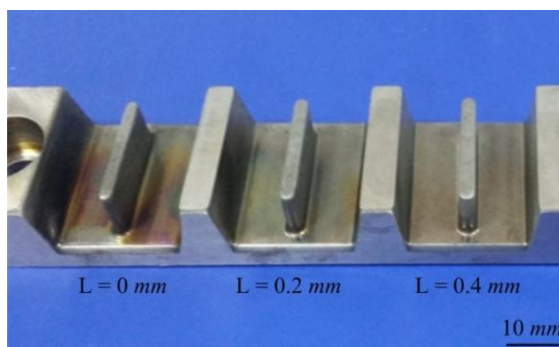


Figure 13. Machined samples of the experiments

In electrochemical trepanning, the blade surface is usually influenced by stray corrosion, so a tapered wall will be formed [18]. A three-coordinate measuring machine was applied to detect the taper of blades fabricated under different protruding length, and the detection scheme is shown in Fig. 14. As is shown in the figure, a line at blade wall is detected. The detect line locates at the middle of blade, and the height deviation Δh is 7 mm. The detection results of taper angle are shown in Fig. 15. As the protruding length L increases from 0 mm to 0.4 mm, the taper angle decreases from 0.286° to 0.106° . Detection result confirms the feasibility of the modified trepanning process with a pictographic insulation sleeve.

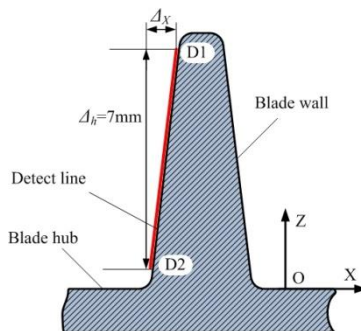


Figure 14. Diagram of the detection scheme

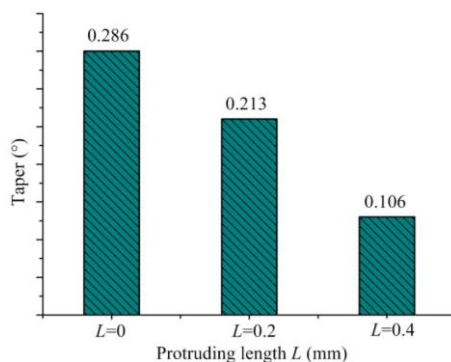


Figure 15. Detection result of blade taper

Surface topography and surface roughness Ra of each blade were also measured by the scanning electron microscope (SEM) and Rtec universal 3D profile meter. The schematic diagram of measurement position is shown in Fig. 16, and the results are shown in Fig. 17. It can be seen from the figure that blades fabricated with different protruding lengths of pictographic insulation sleeve have different topographies. When the protruding length is 0 mm, a rippled surface is formed, and the surface roughness of the blade is up to $1.572 \mu\text{m}$ (Fig. 16a). Gradually, with increase in the protruding length, the blade surface becomes smoother and the surface roughness decreases. When the protruding length is set to 0.4 mm, the surface roughness is limited to $0.907 \mu\text{m}$ (Fig. 16c). Research shows that the stray current can induce corrosion only after a certain time [19]. When the impacted height of stray current is effectively controlled by the pictographic insulation sleeve, the impact time is decreased. So, surface quality of the blade becomes better.

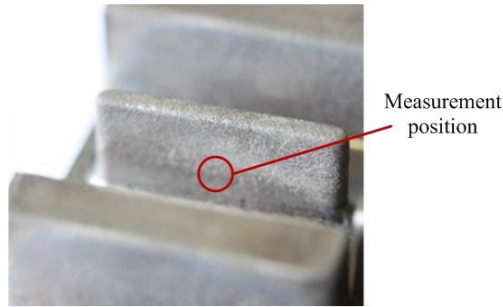


Figure 16. Schematic diagram of the measurement position

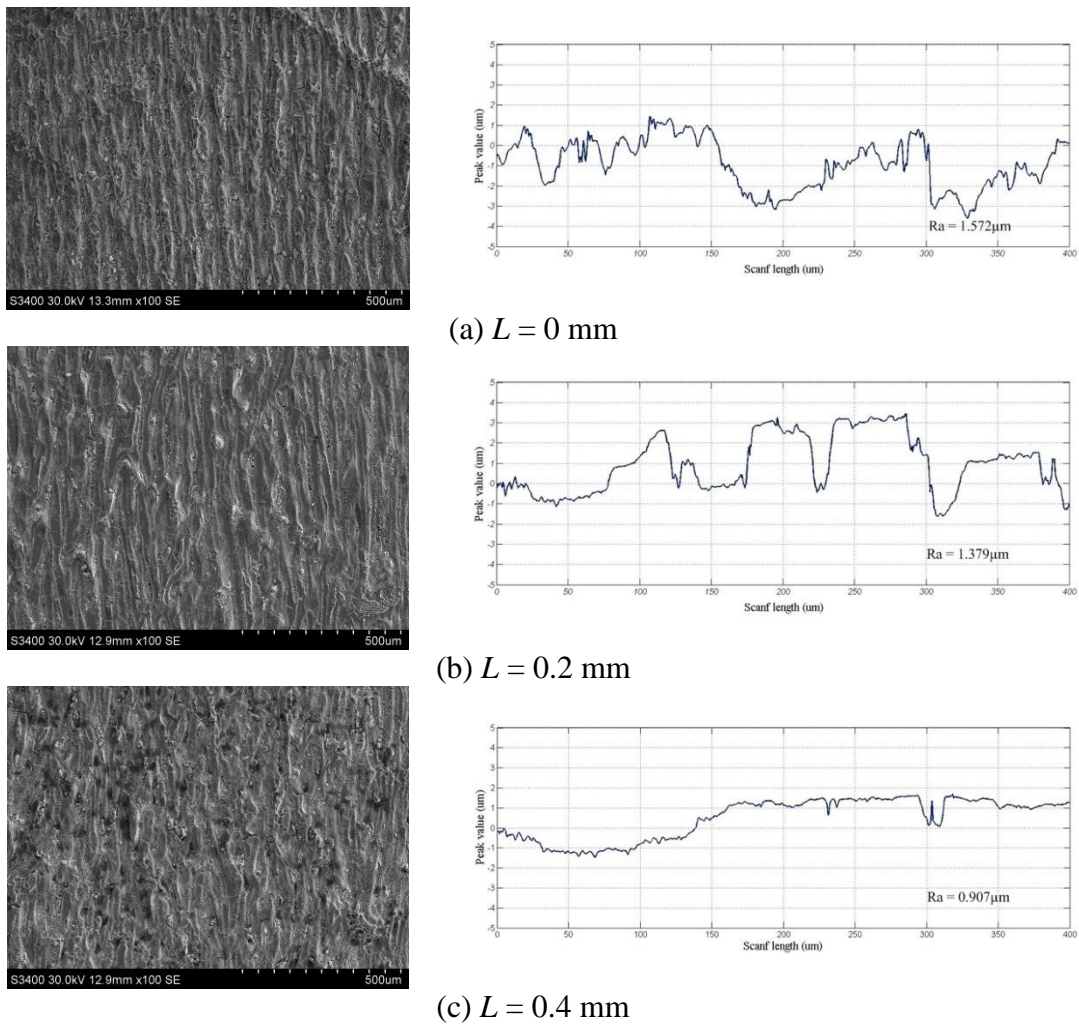


Figure 17. Surface topographies and roughness of the blades fabricated in different conditions

5. CONCLUSIONS

In electrochemical trepanning, stray corrosion is a key problem which influences the machining accuracy of the fabricated blade. In this paper, a modified trepanning process with a pictographic

insulation sleeve was proposed to restrict the impacted height by stray corrosion. A computer-aided optimization method was developed to design the protruding length of the pictographic insulation sleeve. Finally, experiments were conducted to confirm the validity of the modified trepanning process. Results showed that the taper and roughness of fabricated blade were reduced to 0.013mm and 0.907 μm respectively, by the optimized protruding length L of 0.4 mm.

ACKNOWLEDGEMENT

The authors wish to acknowledge the financial support provided by the Key Program of the China Natural Science Foundation (51535006) and the Fundamental Research Funds for the Central Universities (NE 2017003).

References

1. K.P. Rajurkar, D. Zhu, J.A. McGeough, J. Kozak and A.D. Silva, *CIRP. Ann-Manuf. Technol.*, 48 (1999) 567.
2. F. Klocke, A. Klink, D. Veselovac, D.K. Aspinwall, S.L. Soo and M. Schmidt, *CIRP. Ann-Manuf. Technol.*, 63(2014)703.
3. F. Klocke, M. Zeis, A. Klink and D. Veselovac, *CIRP. Ann-Manuf. Technol.*, 6 (2013) 368.
4. B. Bhattacharyya and J. Munda, *Int. J. Mach. Tool. Manuf.*, 43 (2003) 1301.
5. Z.Y. Xu, Q. Xu, D. Zhu and T. Gong, *CIRP. Ann-Manuf. Technol.*, 62 (2013) 187.
6. D. Zhu, C. Liu, Z.Y. Xu and J. Liu, *Chinese. J. Aeronaut.*, 24 (2016) 1111.
7. T. Fujisawa, I. Kazuaki, Y. Makoto and K. Dai, *J. Fluids. Eng.*, 130 (2008) 081.
8. F. Klocke, M. Zeis, S. Harst, A. Klink, D. Veselovac and M. Baumgartner, *Procedia. CIRP.*, 8 (2013) 265.
9. A.N. Zaytsev, V.P. Zhitnikov and T.V. Kosarev, *J. Mater. Process. Technol.*, 149 (2004) 439.
10. D.S. Bilgi and P.V. Jadhav, *Int. J. Comput. Commun. Inform. Syst.*, 12 (2010) 49.
11. M. Burger, L. Koll, E.A. Werner and A. Platz, *J. Manuf. Process*, 14 (2014) 62.
12. C. Rosenkranz, M.M. Lohrengel and J.W. Schultze, *Electrochim. Acta*, 50 (2004) 2009.
13. V.K. Jain, Y. Kanetkar and G.K. Lal, *Int. J. Adv. Manuf. Technol.*, 26 (2005) 527.
14. X.L. Fang, N.S. Qu, Y.D. Zhang, Z.Y. Xu and D. Zhu, *J. Mater. Process. Technol.*, 214 (2014) 556.
15. X.L. Chen, N.S. Qu, X.L. Fang and D. Zhu, *Surf. Coat. Tech.*, 277 (2015) 44.
16. D.Y. Wang, Z.W. Zhu, J. Bao and D. Zhu, *Int. J. Adv. Manuf. Technol.*, 76 (2014) 1365.
17. X.L. Fang, N.S. Qu, H.S. Li and D. Zhu, *Int. J. Adv. Manuf. Technol.*, 68 (2013) 2005.
18. D. Zhu, Z.Z. Gu, T.Y. Xue and A. Liu, *Chinese. J. Aeronaut.*, 30 (2017) 1624.
19. L. Bertolini, M. Carsana and P. Pedferri, *Corrosion. Sci.*, 49 (2007) 1056.

© 2017 The Authors. Published by ESG (www.electrochemsci.org). This article is an open access article distributed under the terms and conditions of the Creative Commons Attribution license (<http://creativecommons.org/licenses/by/4.0/>).